Supporting Information

Outstanding Electrode-Dependent Seebeck Coefficients in Ionic Hydrogels for Thermally Chargeable Supercapacitor near Room Temperature

Shohei Horike[*†‡§], Qingshuo Wei[†§], Kazuhiro Kirihara[†], Masakazu Mukaida[†], Takeshi Sasaki[†], Yasuko Koshiba[‡], Tatsuya Fukushima[‡], and Kenji Ishida[‡‖]*

[†]Nanomaterials Research Institute, National Institute of Advanced Industrial Science and Technology (AIST), 1-1-1 Higashi, Tsukuba 305-8565, Japan

[‡]Department of Chemical Science and Engineering, Graduate School of Engineering, Kobe University, 1-1 Rokkodai-cho, Nada-ku, Kobe 657-8501, Japan

[§]PRESTO, Japan Science and Technology Agency, Kawaguchi 332-0012, Japan

[‖]Research Center for Membrane and Film technology, Kobe University, 1-1 Rokkodai-cho, Nada-ku, Kobe 657-8501, Japan

*Correspondence to: horike.crystal@aist.go.jp

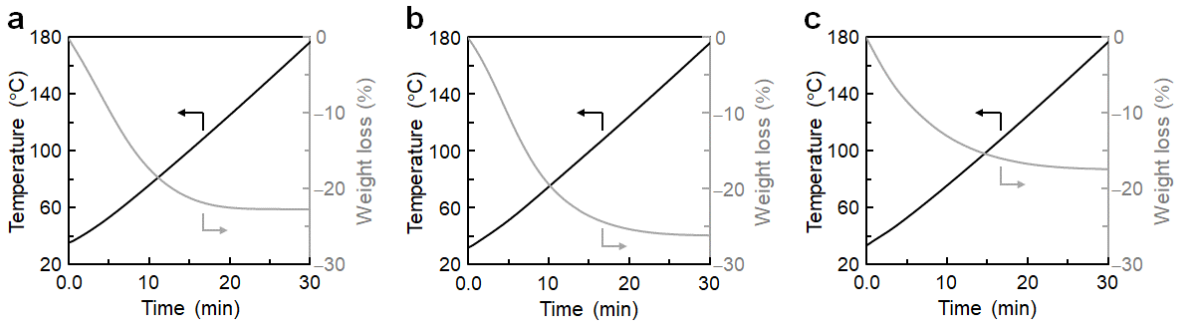

Figure S1. Thermogravimetry (TG) measurement results of hydrogels of a) Emim-Cl, b) Hmim-Cl, and c) Dmim-Cl with PVA. The measurements were performed at a heating rate of 5 °C min^{-1} under N_2 gas flow (200 mL min^{-1}) using a commercial TG setup (TG/DTA 7200 system, Seiko Instruments). Mass reduction of approximately 20% after heating is attributed to the water evaporation and accordingly corresponds to the residual water content in the prepared hydrogels.

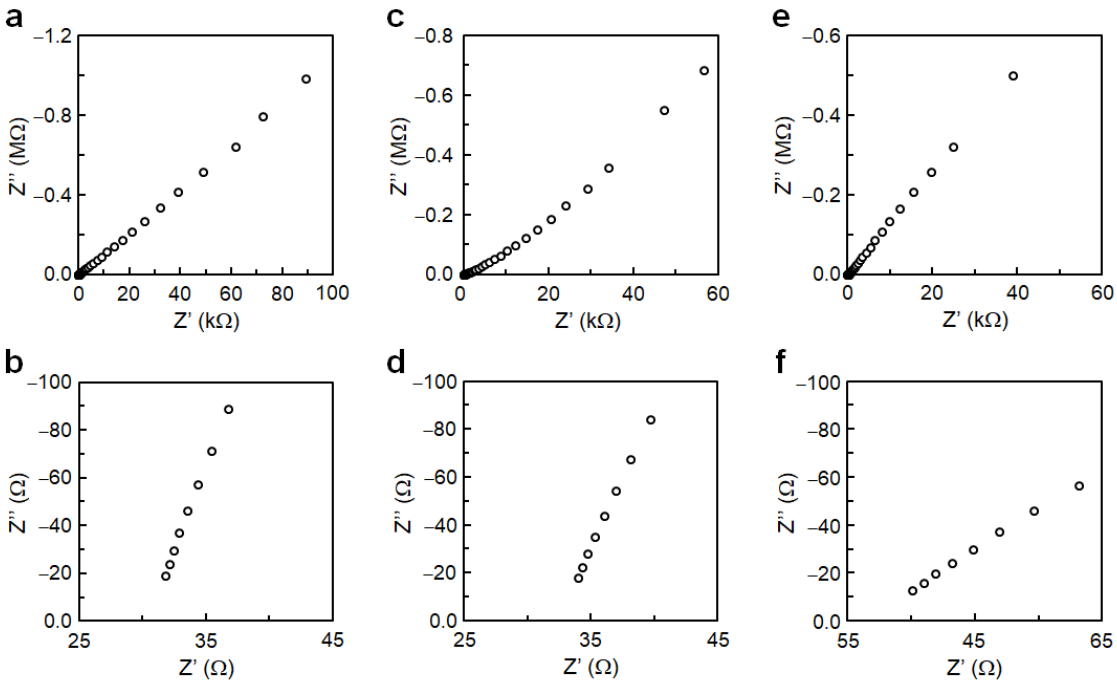

Figure S2. Nyquist diagrams of hydrogels of a,b) Emim-Cl, c,d) Hmim-Cl, and e,f) Dmim-Cl with PVA, measured using F-doped tin oxide transparent electrodes. The lower panels are enlarged views of the upper panels. The series resistances of the gels were determined from the intersection of the fitting curves with the real axes. The plots were suitably fitted by an equivalent circuit consisting of a series resistance and a constant phase element.

Table S1. Representative data for weight-ratio-dependent performance indicators of hydrogels composed of Emim-Cl and PVA.

Emim-Cl/PVA weight ratio	$S^{\dagger}$ (mV K^{-1})	$\sigma_{AC}{}^{\ddagger}$ (mS cm^{-1})
1:1	+4.8	0.65
3:1	+6.4	0.97
6:1	+7.2	1.3
10:1	+10.1	1.6

$^{\dagger}S$: Seebeck coefficient; $^{\ddagger}\sigma_{AC}$: ionic conductivity

Table S2. Comparison of performance indicators of several ionic Seebeck materials. The notation of chemicals used in this table follows the notation used in the original studies.

Ref.	Electrolyte	$S^{\dagger}$ (mV K^{-1})	$\sigma^{\ddagger}$ (mS cm^{-1})	$\kappa^{\S}$ (W m^{-1} K^{-1})
This study	Emim-Cl/PVA/H_2O	+10.1	1.6	0.29
S1	NaCl/H_2O	0.63	–	–
S2	NaOH/PEO	11.1	0.0813	0.216
S3	EMIMTFSI	1.446	8.608	0.085
S4	Polystyrene sulfonic acid	7.9	90	~0.38
S5	EMIM:DCA/PVDF-HFP	26.1	6.7	0.176
S6	Sodium acetate/formamide	3.6	–	–
S7	Tetrabutylammonium nitrate/dodecanol	7.16	0.0117	0.169
S8	NaOH/polyethyleneoxide with cellulosic membrane	24	~20	~0.4

$^{\dagger}S$: Seebeck coefficient; $^{\ddagger}\sigma$: ionic conductivity; $^{\S}\kappa$: thermal conductivity

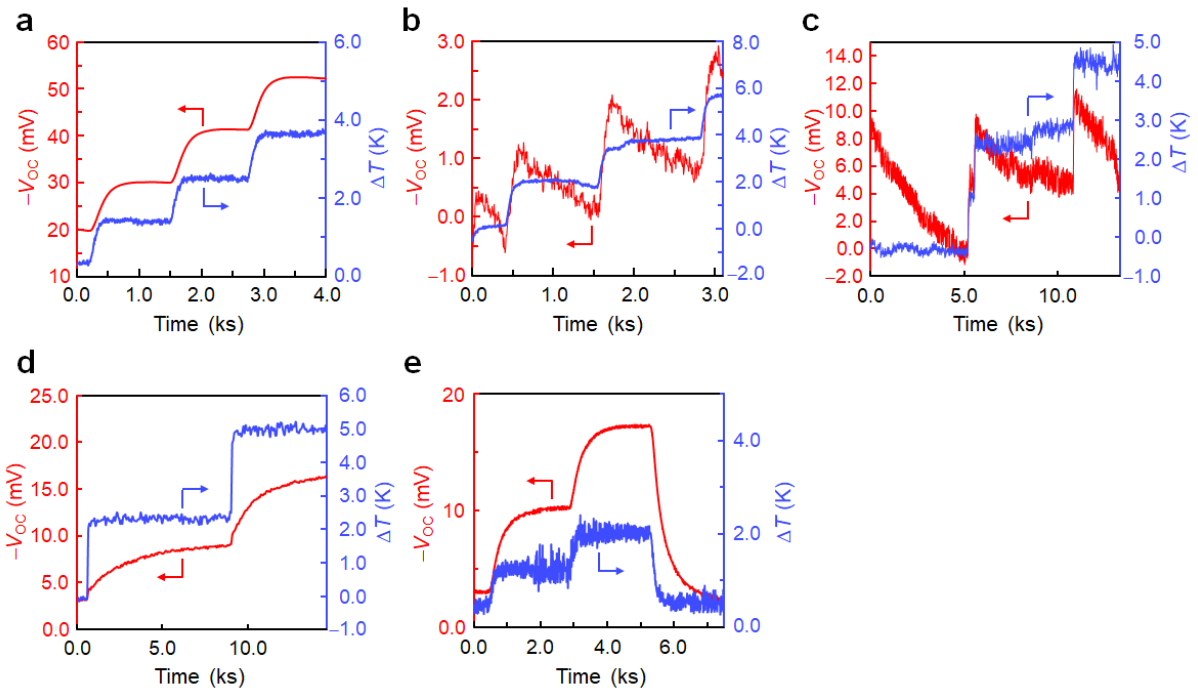

Figure S3. Open circuit voltage responses from Emim-Cl/PVA hydrogels under application of temperature differences measured with a) Ag paste, b) Au foil, c) Ni foil, d) Pt foil, and e) Ag foil electrodes. Among these tests, those with Ni and Au electrodes provided transient voltage response, while stable responses were obtained with Ag and Pt electrodes.

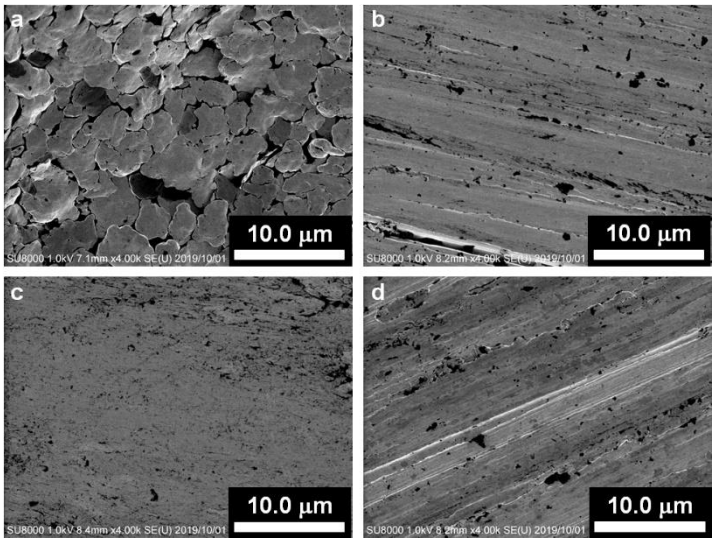

Figure S4. Scanning electron microscopy images of a) Ag paste, b) Ag foil, c) Au foil, and d) Pt foil. Metal foils (Ag, Au, and Pt) have a relatively smooth surface and do not show distinctive character on their surface structures, regardless of the metal type. The Ag paste electrode has a rough surface structure as it is formed by silver nanoparticles, which may be effective for increasing the mean contact area with the electrolytes and decreasing the contact resistance. However, the main contributor to the varied open circuit voltage responses according to the electrodes (Figure S3) is not the surface roughness, but the metal type of the electrodes, because measuring with Ag electrodes provides a stable open circuit voltage response (Figure S3a,e), regardless of the surface structure.

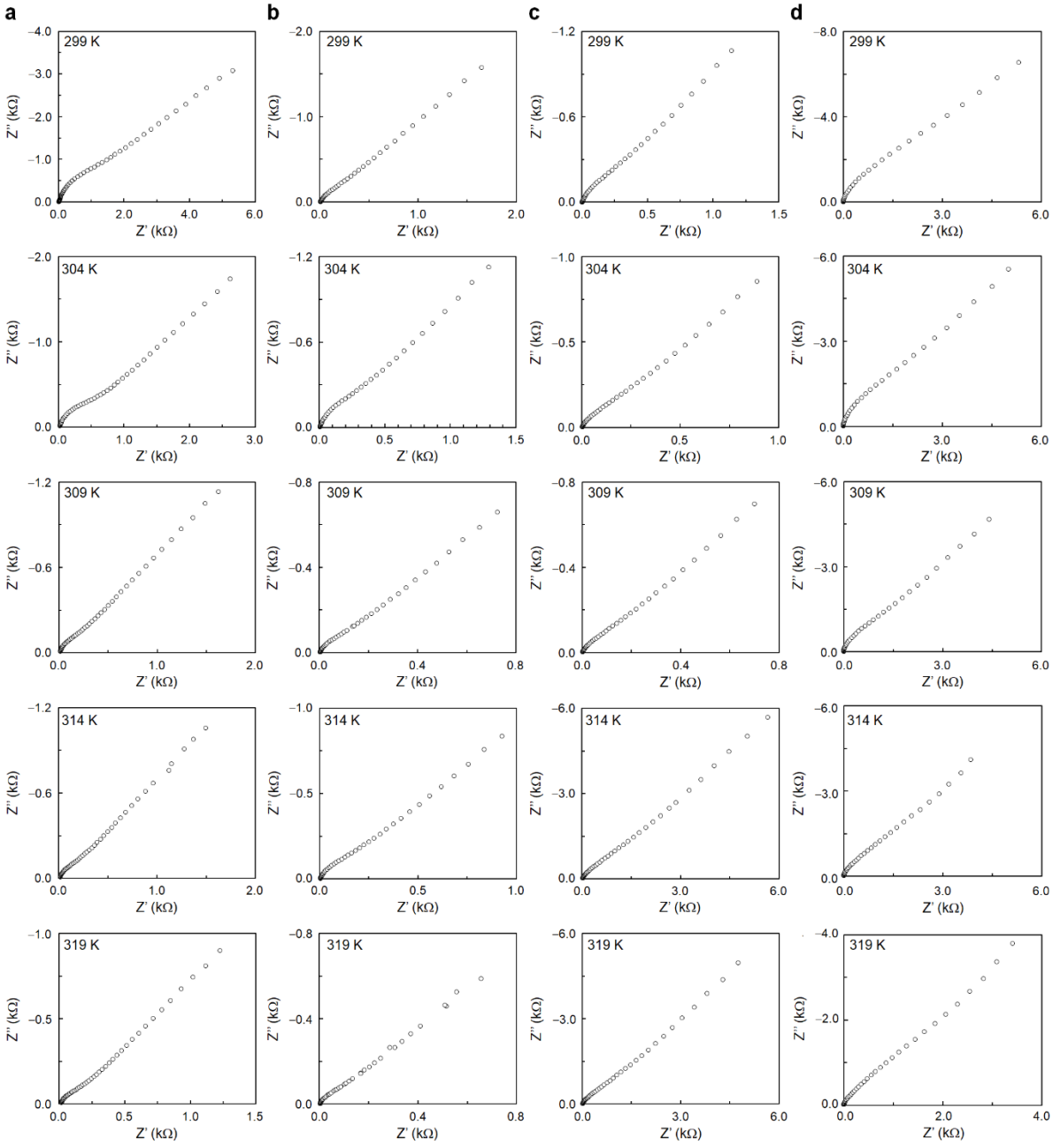

Figure S5. Representative temperature-dependent Nyquist diagrams of a) Emim-Cl/PVA, b) Hmim-Cl/PVA, and c) Dmim-Cl/PVA hydrogels measured by Ag foil electrodes, and d) Emim-Cl/PVA measured by Au foil electrodes.

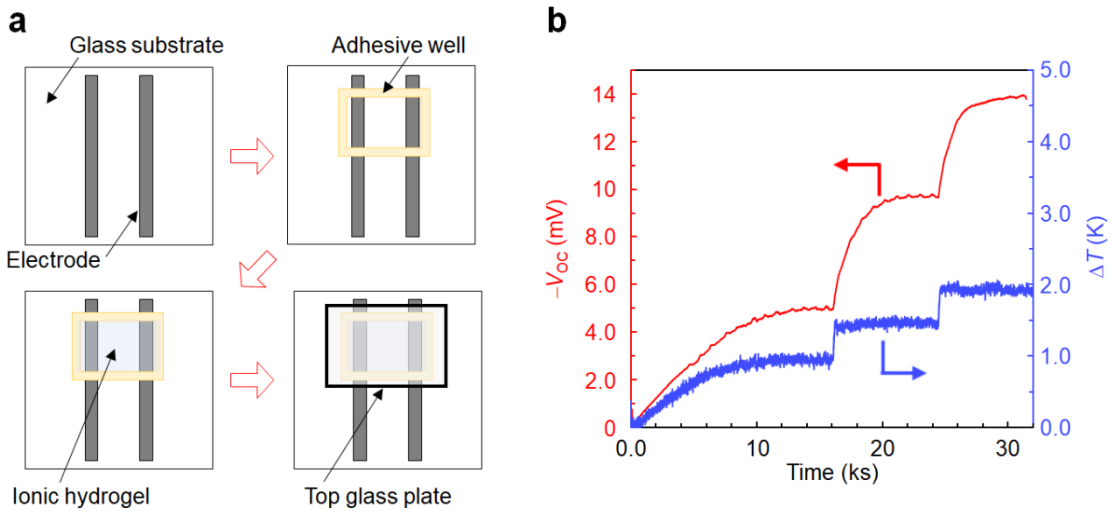

Figure S6. a) Schematic of sealing mechanism using adhesive and a glass plate to suppress water evaporation. b) Open circuit voltage (V_{OC}) response of the sealed Emim-Cl/PVA hydrogel (Emim-Cl/PVA = 10:1) test sample measured using Ag electrodes. The Seebeck coefficient of approximately +9.0 mV K^{-1} was nearly identical to that observed without sealing (*i.e.*, the coefficients shown in the main article), which suggests that the influence of water evaporation on the thermoelectric voltage generation is negligible for our hydrogel.

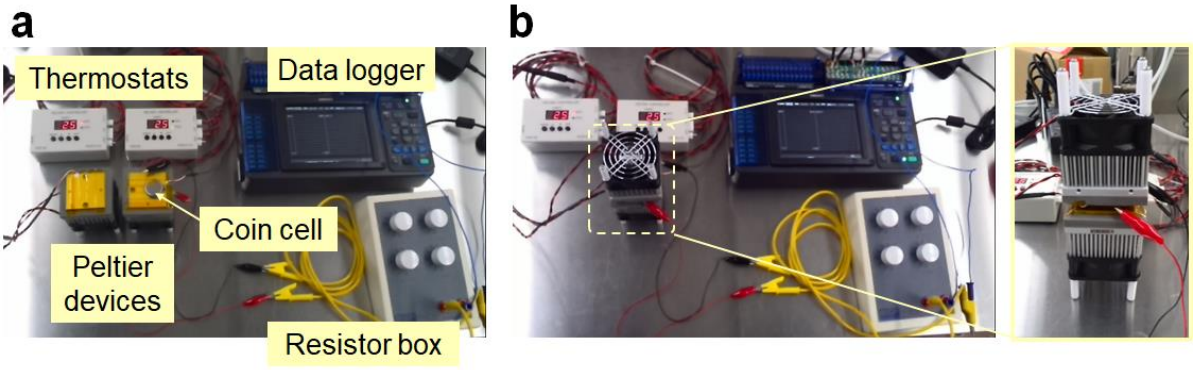

Figure S7. Photographs of measurement setup for voltage response from the coin cell type TE supercapacitor shown in Figure 4a of the main article. a) The setup consists of two Peltier devices that are controlled by thermostats (VPE 20-30S, VICS). The voltage from the TE supercapacitor is measured by a data logger. The load resistance is controlled by a resistor box. b) Upon measurement, the coin cell is put between the two Peltier devices to supply the temperature difference.

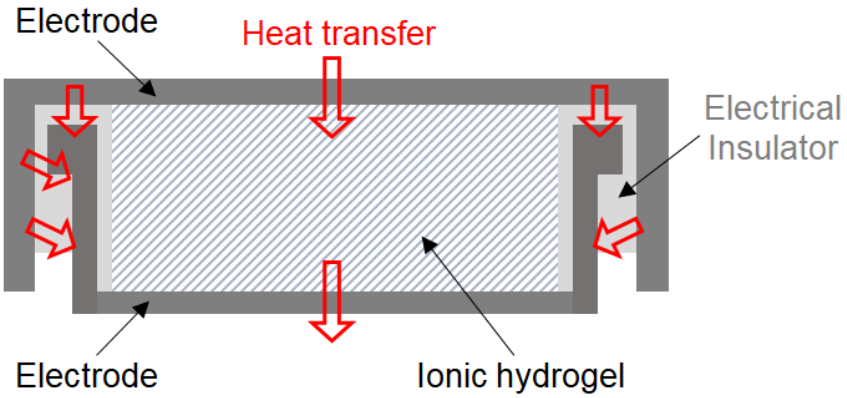

Figure S8. Schematic of the cross-sectional view of the coin cell. The two electrodes are separated by elastomers for insulation. From the viewpoint of thermal design, the heat flow (indicated by red arrows) between the electrodes across the insulator wall does not seem negligible; consequently, the effective temperature difference supplied to the integrated gel is lost over time in the present coin cell structure. For example, as shown in Figure 4c of the main manuscript, the temperature difference (measured on the outer surfaces of the two electrodes) is approximately 7.9 K. Considering the Seebeck coefficient of the hydrogel (10 mV K^{-1}), the open circuit voltage is expected to be on the order of >70 mV; however, the observed open circuit voltage is approximately 9.3 mV. This is quite small for the temperature difference of 7.9 K. Therefore, the effective temperature difference supplied to the inner hydrogel does not correspond to the temperature difference measured on the outer surfaces of the electrodes. Considering the Seebeck coefficient and the observed open circuit voltage, the actual temperature difference supplied to the integrated gel seems to be at most ~0.9 K. Expanding the distance between these electrodes as well as the cross sectional area of the device is one of the practical approaches to ensure a large temperature difference and low electrical impedance.

Table S3. Chemicals and materials list.

Chemical/material	Purity (%)	Supplier	Remark
1-Ethyl-3-methylimidazolium chloride (Emim-Cl)	98	FUJIFILM Wako Pure Chemical	
1-Hexyl-3-methylimidazolium chloride (Hmim-Cl)	92	FUJIFILM Wako Pure Chemical	
1-Decyl-3-methylimidazolium chloride (Dmim-Cl)	95	FUJIFILM Wako Pure Chemical	
Poly(vinyl alcohol) (PVA)	–	FUJIFILM Wako Pure Chemical	
Deionized water	–	AS ONE	Conductivity ≤ 0.1 mS m^{-1}
Ag (paste)	–	FUJIKURA KASEI	Product No. D-550 Used after application and drying at room temperature (~298 K) in air
Ag (foil)	99.98	Nilaco	Product No. AG-403324
Au (foil)	–	TANAKA Precious Metals	Lot No. 5S098-40625 Au foils were prepared by vapor deposition
Pt (foil)	99.98	Nilaco	Product No. PT-353325
Ni (foil)	99	Nilaco	Product No. NI-313253
F-doped tin oxide (FTO) glass	–	AS ONE	Product No. NPV-CFT2-7
Toluene	99.5	FUJIFILM Wako Pure Chemical	Used for dispersing Ag paste

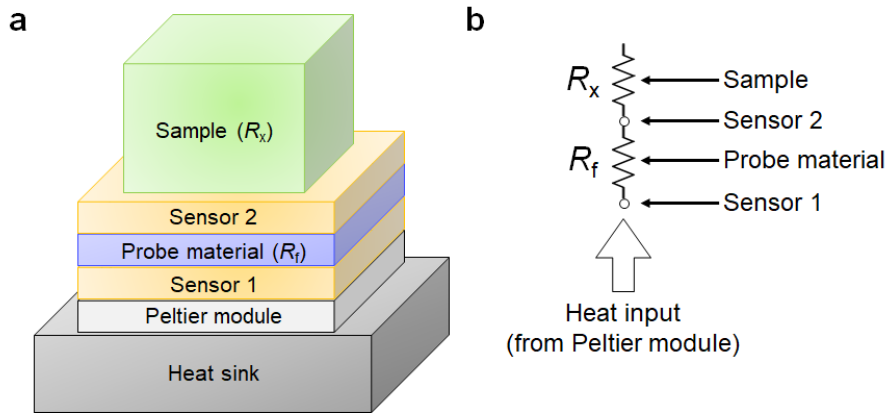

Figure S9. Schematics of a) thermal conductivity measurement system of ai-Phase Mobile M10 and b) equivalent thermal circuit model of the system. A Peltier module is used as a heater, which is placed on a heat sink (aluminum block with a high thermal capacity). A probe material (in this study, polyethylene terephthalate film with a thickness of 500 μm) is put between two thermopiles (sensors 1 and 2) which are constructed from five thermocouples, and then placed on the Peltier module. The gel sample is placed on sensor 2.

To determine the thermal conductivity of the sample, a temperature wave (oscillation) with the frequency of 50 mHz and the amplitude of ±1 °C is generated using the Peltier module. This temperature wave diffuses into the sample after passing through the probe material while the amplitude is decaying. The two sensors read the temperature amplitudes at the front and the back sides of the probe material. Specifically, this measurement process corresponds to monitoring the one-dimensional heat flow across the standard thermal resistance R_f (the probe material) that is connected to the thermal resistance R_x (of the test sample), in series, by exploiting the temperature changes at both sides of R_f. The decay of the temperature amplitude from sensor 1 to 2 is affected by the thermal conductivity of the sample placed on sensor 2. The inverse of the decay ratio of the temperature amplitudes is correspondent to the thermal effusivity of the sample. The thermal effusivity (e) is related to the thermal conductivity (κ) and the specific heat capacity per volume (c) of the test sample as $e = (\kappa c)^{1/2}$; therefore, at this stage, the thermal conductivity cannot be separated from the specific heat capacity. However, according to the Dulong–Petit law, the molar specific heat capacity takes an almost constant value above the Debye temperature, regardless of the material type. Further, if the frequency of the temperature wave is low (*e.g.*, 50 mHz), the change in specific heat capacity is expected to be negligibly small during the measurement. Therefore, if the thermal effusivity values of the other two referential materials with known thermal conductivities (*e.g.*, water, air, or polymer blocks) are obtained by the

same measurement system, the specific heat capacity term can be immediately canceled out from the equation, which is followed by the direct determination of the thermal conductivity of the sample. The actual measurement data is summarized in Table S4 with the decay ratios of the temperature amplitude across the probe material, when referential deionized water and a polymer block are placed on sensor 2.

Table S4. Summary of decay ratio of the temperature amplitude ("gain") and correspondent thermal conductivity of two standard samples (deionized water and porous polyethylene block), including the hydrogel samples obtained by the measurement principle shown in Figure S9. The frequency and temperature amplitude of the temperature oscillation by the Peltier module were set to 50 mHz and ±1 °C, respectively. For the hydrogels, the listed values are the average of nine measurements.

Material	Gain	$\kappa^{\dagger}$ (W m^{-1} K^{-1})
Deionized water (standard material)	0.2282	0.610 (reference value)
Porous polyethylene block (standard material)	0.6573	0.0520 (reference value)
Emim-Cl/PVA hydrogel	0.3614	0.294
Hmim-Cl/PVA hydrogel	0.3683	0.284
Dmim-Cl/PVA hydrogel	0.3928	0.251

$^{\dagger}\kappa$: thermal conductivity

Regarding the TE voltage generation by temperature-dependent electrode potential

In the main article, we discussed a possible mechanism for the electrode-dependent TE voltage generation from the viewpoint of thermally induced ionic polarization at the interface between the electrolyte and the electrodes. Here, we further discuss the other possible mechanism for the voltage generation. If the electrolyte contains both oxidants (Ox) and reductants (Red) and the electron transfer reaction between these is under equilibrium (Ox + z e$^-$ ⇄ Red), the electrode potential (E) will be expressed as follows (Nernst equation):

$$E = E° + \frac{RT}{zF} \ln \frac{a_{\mathrm{Ox}}}{a_{\mathrm{Red}}} \qquad \text{(S1)}$$

where $E°$ is the standard electrode potential, R is the gas constant, T is the temperature, z is the transferred amount of electrons, F is the Faraday constant, and a_i is the activities of Ox and Red. Accordingly, the electrode potential is affected by the temperature. Under a slight temperature difference (dT), the electrode potentials at the high and the low temperatures are written as:

$$E_{T_\mathrm{h}} = E° + \frac{RT_\mathrm{h}}{zF} \ln \frac{a_{\mathrm{Ox}}}{a_{\mathrm{Red}}} \qquad \text{(S2)}$$

$$E_{T_\mathrm{l}} = E° + \frac{RT_\mathrm{l}}{zF} \ln \frac{a_{\mathrm{Ox}}}{a_{\mathrm{Red}}} \qquad \text{(S3)}$$

where T_h and T_l are the high and low temperatures, respectively, ($T_\mathrm{h} > T_\mathrm{l}$), and E_{Ti} is the electrode potentials at these temperatures. Equations (S2) and (S3) should immediately provide the potential difference between these electrodes (d$E = E_{T\mathrm{h}} - E_{T\mathrm{l}}$) per temperature difference (d$T = T_\mathrm{h} - T_\mathrm{l}$), namely, the Seebeck coefficient (S), as:

$$S = -\frac{\mathrm{d}E}{\mathrm{d}T} = \frac{R}{zF} \ln \frac{a_{\mathrm{Ox}}}{a_{\mathrm{Red}}} \qquad \text{(S4)}$$

In the case of Rmim-Cl/PVA hydrogels, any redox couple is not contained. However, the partial electron transfer process between the metal electrode (M) and the anion (A^-) may have to be taken into consideration as: $M + A^- \rightleftarrows M{\cdot}A^{(1-\gamma)-} + \gamma e^-(M)$. Here, γ is the partial amount of transferred electrons. Therefore, the temperature-dependent partial electron transfer would contribute to the TE voltage generation, if this process is under equilibrium, and obey the Nernst equation. This process leaves the surplus electrons (γe^-) in the metal electrodes; and accordingly, the materials should behave like a cell rather than a capacitor under loading of external resistance, because the surplus electrons should continuously flow through the electric circuit. However, our hydrogels exhibited capacitor-like behavior during loading, as shown in Figure 1d of the main

article. Hence, at present, we believe that the thermally induced interfacial polarization mechanism rather than the electron transfer is dominant for TE voltage generation.

References

(S1) Lim, H.; Lu, W. Y.; Chen, X.; Qiao, Y. Anion Size Effect on Electrode Potential in a Nanoporous Carbon. *Int. J. Electrochem. Sci.* **2012**, *7* (3), 2577–2583.

(S2) Zhao, D.; Wang, H.; Khan, Z. U.; Chen, J. C.; Gabrielsson, R.; Jonsson, M. P.; Berggren, M.; Crispin, X. Ionic thermoelectric supercapacitors. *Energy Environ. Sci.* **2016**, *9* (4), 1450–1457.

(S3) Jia, H. Y.; Tao, X. L.; Wang, Y. P. Flexible and Self-Healing Thermoelectric Converters Based on Thermosensitive Liquids at Low Temperature Gradient. *Adv. Electron. Mater.* **2016**, *2* (7), 1600136.

(S4) Kim S. L.; Lin H. T.; Yu C. Thermally Chargeable Solid-State Supercapacitor. *Adv. Energy Mater.* **2016**, *6* (18), 160546.

(S5) Cheng, H. L.; He, X.; Fan, Z.; Ouyang, J. Y. Flexible Quasi-Solid State Ionogels with Remarkable Seebeck Coefficient and High Thermoelectric Properties. *Adv. Energy Mater.* **2019**, *9* (32), 1901085.

(S6) Lim, H.; Shi, Y.; Qiao, Y. Thermally chargeable supercapacitor working in a homogeneous, changing temperature field. *Appl. Phys. A* **2016**, *122* (4), 443.

(S7) Bonetti M.; Nakamae S.; Roger M.; Guenoun P. Huge Seebeck coefficients in nonaqueous electrolytes. *J. Chem. Phys.***2011**, *134* (11), 114513.

(S8) Li, T.; Zhang, X.; Lacey, S. D.; Mi, R. Y.; Zhao, X. P.; Jiang, F.; Song, J. W.; Liu, Z. Q.; Chen, G.; Dai, J. Q.; Yao, Y. G.; Das, S.; Yang, R. G.; Briber, R. M.; Hu, L. B. Cellulose ionic conductors with high differential thermal voltage for low-grade heat harvesting. *Nat. Mater.* **2019**, *18* (6), 608–613.